Structure and dynamics of a predicted ferredoxin-like selenoprotein in Japanese encephalitis virus

By: Haizhen Zhong and Ethan Will Taylor

Abstract:

Homologues of the selenoprotein glutathione peroxidase (GPx) have been previously identified in poxviruses and in RNA viruses including HIV-1 and hepatitis C virus (HCV). Sequence analysis of the NS4 region of Japanese encephalitis virus (JEV) suggests it may encode a structurally related but functionally distinct selenoprotein gene, more closely related to the iron-binding protein ferredoxin than to GPx, with three highly conserved UGA codons that align with essential Cys residues of ferredoxin. Comparison of the probe JEV sequence to an aligned family of ferredoxin sequences gave an overall 30.3% identity and 45.8% similarity, and was statistically significant at 4.9 S.D. ($P < 10^{-6}$) above the average score computed for randomly shuffled sequences. A 3-dimensional model of the hypothetical JEV protein (JEV model) was constructed by homology modeling using SYBYL, based upon a high resolution X-ray structure of ferredoxin (PDB code: 1awd). The JEV model and the model from 1awd were subsequently subjected to molecular dynamics simulations in aqueous medium using AMBER 6. The solution structure of the JEV model indicates that it could fold into a tertiary structure globally similar to ferredoxin 1awd, with RMSD between the averaged structures of 1.8 Å for the aligned regions. The modeling and MD simulations data also indicate that this structure for the JEV protein is energetically favorable, and that it could be quite stable at room temperature. This protein might play a role in JEV infection and replication via TNF and other cellular stimuli mediated via redox mechanisms.

Keywords: Homology modeling | Sequence analysis | Molecular dynamics | Ferredoxin | Japanese encephalitis virus

Article:

1. Introduction

The flavivirus family (Flaviviridae) consists of three genera: the pestviruses; the hepaciviruses, to which belongs hepatitis C virus (HCV); and the flaviviruses. Worldwide, over 140 million

people, more than four times the number of HIV-positive individuals, are chronically infected with HCV. In addition to HCV, major human pathogens among the flaviviruses include Japanese encephalitis virus (JEV), dengue fever virus (DENV), yellow fever virus (YFV), and West Nile virus (WNV).

JEV is well known as the causative agent of Japanese encephalitis, a potentially serious inflammatory disease of public health concern, associated with significant mortality in many Southeast Asian countries. JEV virus is a small enveloped virus containing a positive-strand RNA genome of approximately 11 kb. The genome is translated as a long open reading frame encoding a polyprotein which can be cleaved post- and co-translationally to generate 10 proteins in the gene order 5′-C-prM-E-NS1-NS2A-NS2B-NS3-NS4A-NS4B-NS5-3′. Among these 10 proteins, the capsid protein C, the premembrane protein prM and the envelope protein E are structural proteins, while NS1 to NS5 proteins represent nonstructural proteins. Much research has been focused on functions of nonstructural proteins NS1, NS2A, NS2B, NS3, NS5 and NS4A. The structure and function of NS4B coding region, however, has received relatively little attention and its function is poorly understood [1].

Progresses in uncovering the links between JEV infection and levels of tumor necrosis factor (TNF) are summarized as follows. Evidence for the role of oxidative stress in JEV infection arose initially from observations that TNF levels are elevated in the serum and in the cerebrospinal fluid of laboratory-confirmed cases of JEV infection [2]. These TNF levels further correlate with JEV-associated mortality. TNF, other pro-inflammatory cytokines such as interleukin 1 and 6, and reactive oxygen species (ROS) have been closely linked with pathology in a wide range of diseases involving an inflammatory basis [3]. The potential damage of the combined effect of ROS and cytokines on the host can be partially inhibited by various antioxidants, including *N*-acetyl cysteine [4], alpha-lipoic acid [5], and selenium (Se) [6]. Selenium is an essential trace element that has many critical functions in mammals, including antioxidant protection, thyroid action, and immune function [7]. Many biological functions of Se are mediated via selenoproteins that contain a selenocysteine as an active site residue [8]. Selenocysteine is encoded, under specific circumstances, by the UGA codon, which otherwise usually serves as a stop codon. Both prokaryotic and eukaryotic organisms encode selenocysteine-containing proteins, using distinct but clearly related co-translational mechanisms for recoding the UGA codon as a sense codon for selenocysteine. Selenoproteins are mostly oxido-reductases, including glutathione peroxidases. The possibility of virally-encoded selenoproteins has now been firmly substantiated in the case of an HIV-1 encoded GPx gene and in the pox virus *Molluscum contagiosum* [9]. The open reading frame (ORF) in *M. contagiosum* contains an in-frame UGA codon, and is highly homologous (76% identical) to mammalian GPx. This ORF was later shown to encode a functional GPx enzyme [10].

In addition to TNF level and the antioxidant implications, the iron level has also been shown to play a role in some flavivirus infections. During HCV infection, iron deposition has been observed to increase, promoting free-radical-mediated lipid peroxidation, and thereby contributing to liver damage and activation of glutathione turnover, whereas reduction of iron levels by phlebotomy appears to have clinical benefits [11]. In JEV infection, redistribution of bodily iron has been reported, with depression of serum iron levels and iron accumulation in the

spleen [12]. Based on all these observations, research on the role of redox regulation in JEV replication is warranted.

In this report, we present our investigation of the potential structure and function of the poorly understood NS4B gene of JEV. We also try to explain the possible roles of this gene in flavivirus replication and pathogenesis, which may be particularly relevant to the observations reviewed above regarding the roles of iron, TNF and ROS in flavivirus infections. This analysis arose out of our previous studies of HCV, where the overlapping −1 reading frame of the NS4 region was shown to encode a homologue of the selenoprotein glutathione peroxidase (GPx) [13]; the same gene was recently identified in HIV-1 and shown to encode a functional GPx enzyme [14]. We will demonstrate in this paper that the analogous JEV NS4B region appears to encode a structurally related but functionally distinct selenoprotein gene, more closely related to the iron-binding protein ferredoxin than to GPx. We have tentatively named this flavivirus gene NS4-fs, referring to the actual or virtual frameshift required to access this reading frame, which in theory could be expressed by various mechanisms, including ribosomal frameshifting, RNA editing, or initiation at an internal start codon in the −1 frame. This mode of encoding suggests that at least part of the function of the zero-frame NS4B protein is to serve as a "spacer" or connection domain, enabling the critical downstream NS5 region to be efficiently translated, despite the low level of production of full length NS4-fs mandated by the inefficiency of initiation of protein synthesis in the overlapping frame, as well as the low cellular levels of selenocysteine, since NS4-fs appears to encode a selenoprotein. Hence, the possibility that a novel selenoprotein may be encoded overlapping the NS4 region of JEV merits serious consideration.

2. Computational methods

2.1. Comparative sequence analysis

All sequence analysis was done using the GCG software package (now part of Accelrys) as well as genome analysis tools [15] and databases provided by the National Center for Biotechnology Information (NCBI); URL: http://www.ncbi.nlm.nih.gov [16]. All JEV sequences used were extracted from GenBank using the StringSearch program of GCG, where only complete genomic sequences were selected for inclusion in the study. These 15 full genomic sequences are: GenBank access numbers #af014160, #af014161, #af069076, #af098736, #af098735, #d90194, #m55506, #u14163, #u15763, #u47032, #d90195, #af075723, #m18370, #l48961, and #af080251. The NS4 coding regions of all these sequences were then aligned using the PileUp program of GCG (Fig. 1S in supplemental materials). Three closely spaced in-frame TGA codons are conserved in all sequences. The coding nucleic acid sequences were translated into peptide sequences by the Translate program of GCG, using an edited translation table to identify the TGA codon as potential encoding selenocysteine [17]. The translated protein sequences were then aligned by PileUp (Fig. 2S in supplemental materials).

The translated JEV #af014160 was selected as a representative sequence for this hypothetical NS4-fs protein to search the nr (non-redundant GenBank) database using the Blastp program. In both database searches and pairwise sequence alignments, cysteine was used in place of selenocysteine in the probe sequence, because the amino acid similarity matrices in common use do not include selenocysteine. After identifying ferredoxin as a homologue, a family of related

ferredoxin sequences were extracted from GenBank and aligned to identify conserved residues pattern and the secondary structure both in ferredoxin family and in the hypothetical NS4-fs protein. The alignment between the query sequence #af014160 and ferredoxin family was carried out using the BestFit program in GCG with subsequent minor manual adjustments (Fig. 1).

```
af014160          MASRSTQSCPEKDSGWNN--EEC-----RCURNGRHUCAUTGKDHSSDAK
                  :||  |||  |     :  ||        :|| |  |: | ||  | : :
   awd    YKVTLKTPSG--EETIECPE-DTYILDAAEEAGLDLPYSCRAG-ACSSCAGKVESGEVD
   a70    AAYKVTLVTPTGNVE--FQCPD-DVYILDAAEEEGIDLPYSCRAG-SCSSCAGKLKTGSLN
   dox    ASYTVKLITPDG--ESSIECSD-DTYILDAAEEAGLDLPYSCRAG-ACSTCAGKITAGSVD
   doy    ASYTVKLITPDG--ESSIECSD-DTYILDAAEEAGLDLPYSCRAG-ACSTCAGKITAGSVD
   roe    ATYKVTLVRPDGS-ETTIDVPE-DEYILDVAEEQGLDLPFSCRAG-ACSTCAGKLLEGEVD
   frd    ASYQVRLINKKQDIDTTIEIDE-ETTILDGAEENGIELPFSCHSG-SCSSCVGKVVEGEVD


af014160 ESRTGAPHRGKRGSVPRQPQCHHCERSRGVGDGAYAHFVGQWSQCRLEFHH  CHGTL
         :|:      :  :        |      ||               :| :| |
   awd   QSDQSFLDDAQMGK-GFVLTCVAYPTS---------------DVTILTHQEAALY
   a70   QDDQSFLDDDQIDE-GWVLTCAAYPVS---------------DVTIETHKKEELTA
   dox   QSDQSFLDDDQIEA-GYVLTCVAYPTS---------------DCTIETHKEEDLY
   doy   QSDQSFLDDDQIEA-GYVLTCVAYPTS---------------DCTIETHKEEDLY
   roe   QSDQSFLDDDQIEK-GFVLTCVAYPRS---------------DCKILTNQEEELY
   frd   QSDQIFLDDEQMGK-GFALTCVTYPRS---------------NCTIKTHQEPYLA
```

Fig. 1. Sequence alignment of query sequence af014160 vs. a family of iron–sulfur ferredoxin proteins. The JEV sequence #af014160 was translated from the af014160 nucleotide sequence. Amino acid code U stands for selenocysteine, Sec, encoded by the UGA codon. Amino acid identities are indicated as (|), and similarities by (:). The alignment was produced using the PileUp and BestFit programs in GCG. The percentage of identity for paired residues is 30.3% and similarity 45.8%. The similarity for this alignment is 4.9 S.D. above the average score computed for 100 optimally aligned randomly shuffled sequences of identical composition.

The similarity of the query sequence #af014160 to the aligned set of ferredoxin sequences (Fig. 1) was further assessed by a variation on the standard method for comparing two sequences, using an in-house computer program, BlockAlign (W. Zhang, J. Kececioglu, E.W. Taylor, unpublished). This program was previously used to assist the sequence analysis during building the HIV-1 GPx model [14]. In brief, the program produces an optimal alignment of the probe sequence (#af014160) compared with a fixed multiple alignment (ferredoxins), by optimizing a scoring function that correctly takes into account linear gap penalties in the multiple alignment. Then the probe sequence is randomly shuffled (100 times in this case), and realigned by the same algorithm. The average alignment score and the standard deviation (S.D.) for random sequences of identical composition are then calculated, and the significance of the actual score is expressed as a Z score (i.e., the number of S.D. from the "expected" random score).

2.2. Model building

The initial model was constructed and minimized on a Silicon Graphics Octane workstation using the SYBYL software package (version 6.7; Tripos Inc., St. Louis, MO) [18]. The template crystal structure of ferredoxin [Fe2S2] was extracted from the Protein Data Bank (PDB id: 1awd) with resolution of 1.4 Å [19].

Based on the alignments in Fig. 1, homology model of NS4-fs (called JEV model hereafter) was constructed using the *biopolymer* module in SYBYL. The small insertions and deletions were handled with *loop_search* module in SYBYL, which uses a knowledge-based approach to rebuild regions where insertions and deletions occur. Insertions and deletions were both handled by deleting one or more residues on either side of the affected region, and by building a new loop that included those anchor residues, plus or minus the required number of residues (e.g., for a single residue insertion, delete 2, rebuild 3). For inserted amino acids, their secondary structures were predicted and accordingly assigned, using the *Qian_Sejnowski* algorithm in SYBYL. The *loop_search* module was invoked wherever insertions and deletions were involved to limit the small changes within the local regions. Annealing was carried out after modeling all deletions and insertions. The resulting models were further refined by molecular mechanics, using the Kollman all-atom force field as implemented in SYBYL. The [Fe2S2] cluster was treated as a rigid aggregate and was deleted from the proteins and the four sulfur atoms from the coordinated cysteine residues were treated as an aggregate. The JEV model was built using Cys in place of selenocysteine since there were no appropriate parameters for selenocysteines coordinated to irons.

In addition to building the JEV model, we also carried out the same molecular mechanics procedures to the 1awd structure (called the AWD model hereafter). After initial optimization in SYBYL, the AWD model and the JEV model were subjected to further energy minimization using the AMBER 6 package [20] with the Cornell et al. all-atom force field [21]. The belly option with ibelly = 1 was used to freeze the movements of the coordinates of the four cysteine residues bound to the [Fe2S2] cluster. The minimizations were implemented with the steepest descent method for the first 500 steps, followed by the conjugate gradient method until the RMS of gradient less than 0.05 kcal/(mol Å).

2.3. Molecular dynamics

In order to observe the stability and dynamic behaviors of the JEV model and the AWD model, both models were subjected to further molecular dynamics (MD) simulations. The SANDER_CLASSIC module of the AMBER 6 package was used in the present study. Both systems were solvated by a cubic box of TIP3P waters [22] which extended at least 12 Å away from any given protein atom. A total of 4671 TIP3P water molecules was added around the AWD model and 5206 was added around the JEV model, with box sizes of approximately 200,785 Å^3 for the AWD model system and 223,400 Å^3 for the JEV model system. System setup for simulations includes the particle mesh Ewald (PME) method for the long-range electrostatics [23], a 10 Å cutoff for nonbonded van der Waals interactions, and periodic boundary conditions. All bonds involving hydrogen atoms were constrained using the SHAKE algorithm in AMBER 6. Constant temperature and pressure (300 K/1 atm) were maintained using the Berendsen coupling algorithm with time constant for heat bath coupling of 0.2 ps [24]. The time step of 2 fs was used to integrate the equations of motion.

Before starting the production-run phase, the following equilibration protocol was applied to both systems. First, the solute molecules were minimized for 500 steps using the steepest descent algorithm while holding water molecules frozen, followed by minimization of water for 500 steps while holding the solute frozen. Subsequently, the whole system was subject to 500 steps

of minimization to remove close contacts and to relax the system. Finally, the whole system was subjected to a gradual temperature increase from 10 to 300 K in six intervals over 30 ps. The whole system was then equilibrated for 100 ps, followed by another 700 ps of MD production phase. The resulting trajectories were analyzed using the PTRAJ module and the CARNAL module of AMBER 6. All simulations were carried out on a SGI-Octane2 workstation. Coordinates were saved every 1 ps for a total of 700. The averaged structures from 700 ps MD simulations for both models were subsequently minimized with a RMS gradient of 0.05 kcal/(mol Å). We analyzed the minimized AWD model and the minimized JEV model using MOE [25] and UCSF MidasPlus [26]. The RMSD between these two models was calculated from the aligned region using UCSF MidasPlus. The root-mean-square deviations (RMSD) of the α-carbons of these two molecules over 700 ps time space were derived using PTRAJ module.

The coordinates of the predicted JEV model are available upon request from the author (wtaylor@rx.uga.edu).

3. Results and discussion

In order to investigate the structure and function of the hypothetical protein encoded in the −1 reading frame of the NS4 region of JEV, 15 full genomic JEV sequences were selected from GenBank. Alignment of these sequences reveals three in-frame UGA codons, which potentially encode selenocysteine. These UGAs are conserved in all 15 sequences (Fig. 1S in supplemental materials). Approximately 60 nucleotides upstream of the first in-frame UGA codon we identified a conserved ATG start codon in the context of a Kozak-like sequence GCTCCCTGGATGG, which is substantially similar to the ideal Kozak sequence GCCGCCRCCATGG. The existence of a Kozak sequence significantly increases the probability that a start codon can serve as a start signal, suggesting that an internal ribosomal entry might be utilized to express this protein. Translation of a peptide sequence beginning from the ATG in the observed Kozak context to the first non-UGA stop codon yields a peptide sequence of 104 amino acids, including the three predicted selenocysteine residues (Fig. 2S in supplemental materials). The translated protein sequence from JEV isolate af014160 was selected as a representative probe sequence and searched against the non-redundant (nr) database at NCBI using the Blastp program. This search yielded ferredoxin as a highly significant hit. In addition, we used the peptide sequence of JEV isolate af014160 as a probe for the protein threading program in MOE and the ferredoxin was the sixth highest hit.

To further explore the possibility that NS4-fs might be a ferredoxin homologue, the alignment of the probe af014160 NS4-fs peptide sequence to an aligned family of ferredoxin sequences was performed, revealing an overall 30.3% identity and 45.8% similarity (Fig. 1). Using the aligned regions of Fig. 1, with a PAM250 comparison matrix, the BlockAlign score for the probe sequence af014160 against the family of ferredoxins is 4.9 S.D. above the average score computed for 100 optimally aligned randomly shuffled sequences of identical composition. Assuming a normal distribution of random scores, this corresponds to highly significant $P < 10^{-6}$. Considering the conservation of critical residues in the active site region, these sequence analysis results suggest the possibility of homology between the probe sequence and ferredoxin. A homology model based on this alignment should be particularly revealing because of the

presence of several significant insertions and deletions in the viral sequence relative to ferredoxin; if the model is not structurally feasible, the apparent sequence similarity might not be functionally significant.

The initial model was built in SYBYL based on the sequence alignment in Fig. 1. Energy optimization for both the JEV model and the AWD model was performed using AMBER 6 with belly option to keep the coordinates of four cysteine residues frozen. These four cysteine residues being restrained in the JEV model are: Cys25, Cys31, Cys34, Cys65, while in the AWD model: Cys37, Cys42, Cys45, and Cys75. Molecular mechanics energy for the restrained in vacuo JEV model is −7992.79 kcal/mol, for the restrained in vacuo AWD model, −6159.17 kcal/mol. The optimized model was subject to unrestrained MD simulation for 700 ps and the averaged structure for the 700 snapshot structures taken from the simulations was derived using PTRAJ module in AMBER 6. Geometry optimization (without constraints) for the average structure from both models gives the total energy for the unrestrained JEV model of −3513.05 kcal/mol, and for the AWD model, −1904.53 kcal/mol. The averaged total energy for each residue for the constrained JEV model is −79.1 kcal/mol; for the constrained AWD model, −65.5 kcal/mol; for the unconstrained JEV model, −34.8 kcal/mol; and for the unconstrained AWD model, −20.3 kcal/mol. These data suggest that in both cases the JEV model is energetically stable.

In order to study the stability of the JEV model in solution we carried out MD simulations for both the JEV model and the AWD model. The equilibrated systems of both AWD model and JEV model were found to be stable under NPT (constant temperature and constant pressure) conditions. The density of the system fluctuates at 1.008 g/cc during the post-equilibration period of simulation. RMS fluctuations during dynamics simulation are often used as an indication of the stability of inter- and intra-domain movements in the protein systems. The RMSD of α-carbons from the initial position ($T = 0$ ps) have been used to measure the stability of the simulations and therefore to provide insight into possible structural fluctuations. Small fluctuations in the RMSD of α-carbons from the averaged structure over the dynamic period are considered as an indication of stable secondary structure. The atom-positional RMSDs of the AWD model and JEV model systems are shown in Fig. 2. The RMSDs of the α-carbons in the JEV model (comparison with the initial structure, $T = 0$ ps, black line in Fig. 2A) stabilized from 100 ps with small variations afterward. This indicates that the apo-JEV model is quite stable over the simulation time. Similarly, the AWD model also maintains stable trajectories during the simulations. However, the AWD model shows bigger fluctuations along the trajectory (magenta line in Fig. 2A), although the RMSDs comparison with $T = 0$ ps for the AWD model is smaller than that for the JEV model. This might indicate that it takes longer for the homologous JEV model to reach a stable conformation and that once the JEV model reaches stable conformations it is quite stable during the rest of the dynamics run. These observations are also in very good agreement with the RMSDs for the averaged structures. The RMSDs for the averaged structures again show that AWD model (blue line in Fig. 2B) experiences more structural fluctuations than the JEV model (magenta line in Fig. 2B). The small RMSDs relative to the averaged MD structure for both models (less than 0.7 Å, Fig. 2B) suggest that the secondary structures in both models are quite stable over the 700 ps MD simulations. The RMSDs for the α-carbons between the AWD model from the MD simulation and the crystal structure are around 1.1 Å (green line in Fig. 2A) and are in harmony with the RMSDs for AWD model to $T = 0$ ps structure. The small

RMSD for the AWD model in comparison to the crystal structure suggests we have a stable and reliable MD simulation.
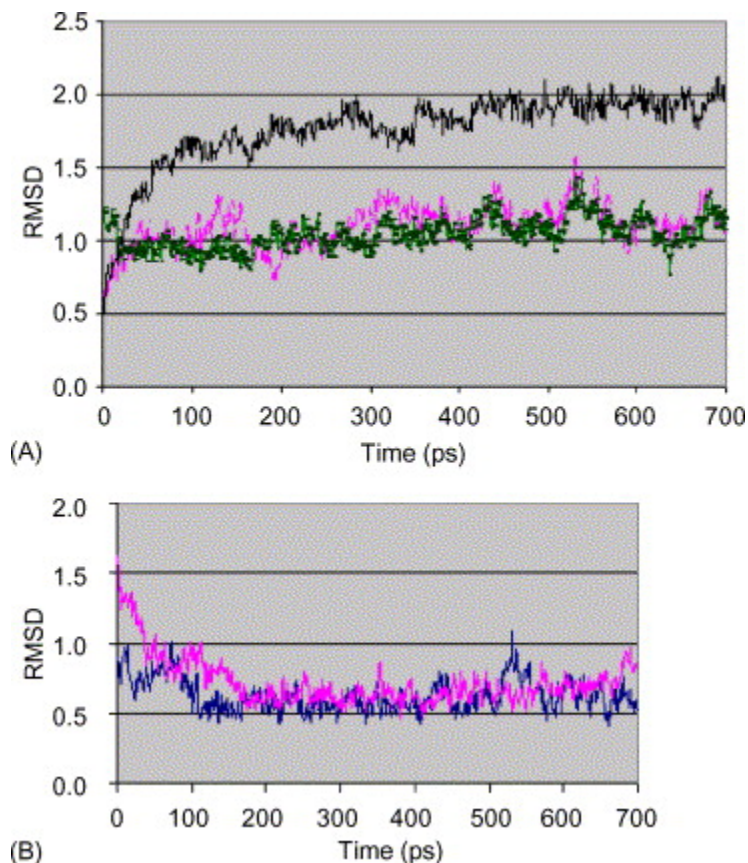

Fig. 2. The RMSDs of the α-carbons from AWD model and from JEV model over the dynamics time space. (A) The blank line represents the JEV model relative to $T = 0$ ps, while the magenta line for the AWD model against the $T = 0$ ps snapshot, and the green line for the AWD model against the averaged structure. (B) The magenta line stands for the JEV model against the JEV averaged structure from MD simulations, while the blue line for the AWD model against its averaged structure.

Comparison of the JEV model and the AWD structure (Fig. 3) shows that overall the homology model of the hypothetical JEV protein is structurally very similar to the template AWD model. The ferredoxin structure is composed of four long β-strands and two small α-helices. Fig. 3 shows not only the β-sheets but also the α-helices are preserved in the model. The RMSD for the α-carbons in the aligned regions between the JEV model (orange in Fig. 3) and the AWD model (green in Fig. 3) for the averaged structure from MD simulations is 1.83 Å. This very good RMSD value supports the proposed homology. Although there is a large insertion for residue 71–87 in the JEV model, these residues were predicted to adopt a random coil according to the secondary structure prediction methods in SYBYL and therefore these residues were built into a random coil, connecting β-strand 3 to β-strand 5. Analysis of the averaged structures from MD simulations of the NS4-fs model and ferredoxin also support the structural similarity.
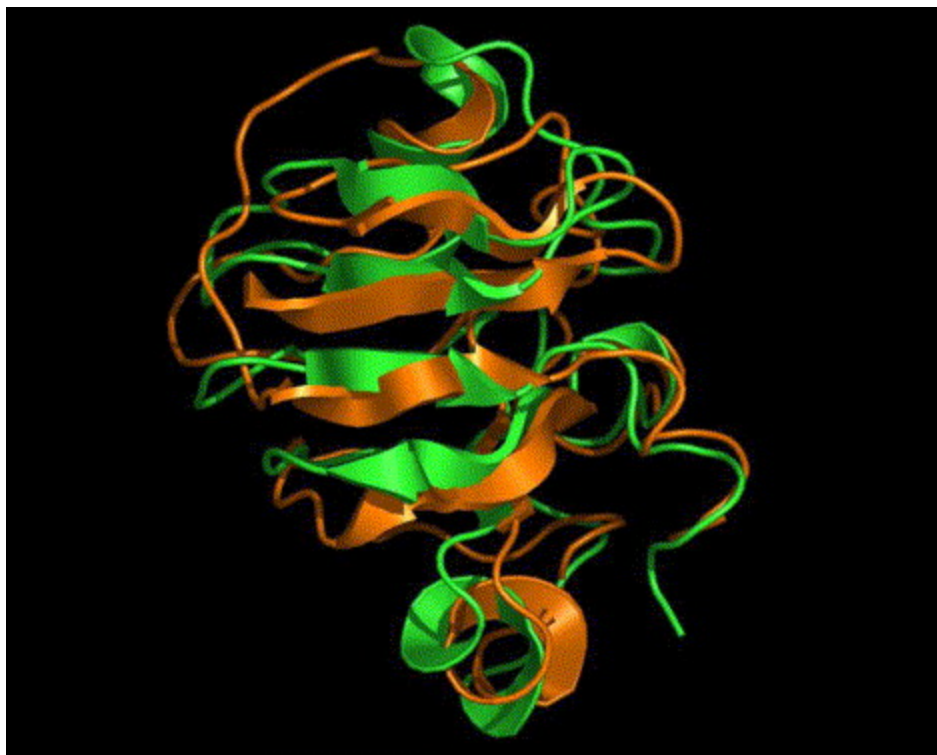
Fig. 3. Backbone structures of both JEV model (orange) and the reference AWD model (green).

To examine the critical [Fe2S2] redox center, which is bound to the protein by interactions between the iron atoms and four cysteine sulfur atoms, we measured the distances between sulfur atoms in the cluster center. Analysis of the cluster-bound regions indicates the JEV model would be quite stable in solution and maintain the geometry of the [Fe2S2] cluster center while the AWD model seems more flexible (Fig. 4). In the MD-derived averaged structure of AWD model, residue Cys37, one of the four cysteines bound to [Fe2S2] cluster, flips away from the crystal structure position. This structural change results in an extended distance between sulfur atoms from Cys37 and Cys45, from original 6.59 to 8.66 Å. The distance between Cys37 sulfur and Cys75 sulfur changes from original 5.16 to 7.06 Å (Table 1). These geometry changes might be vital because they happen within the [Fe2S2] redox center. This indicates that in the absence of the [Fe2S2] cluster, the clustering cysteine residues (residues in magenta in Fig. 4) are quite flexible in the AWD model in water medium. On the contrary, the distances between any sulfur atoms combinations from four bound cysteines in the JEV model (residues in yellow in Fig. 4) fall into the allowable variations from the original data in the crystal structure. This strongly suggests that the hypothetical JEV protein would be quite stable during MD simulations. Combining these observations with energetic data as well as the RMSDs values, one could conclude that the JEV model should be dynamically stable as well as structurally and energetically favorable.
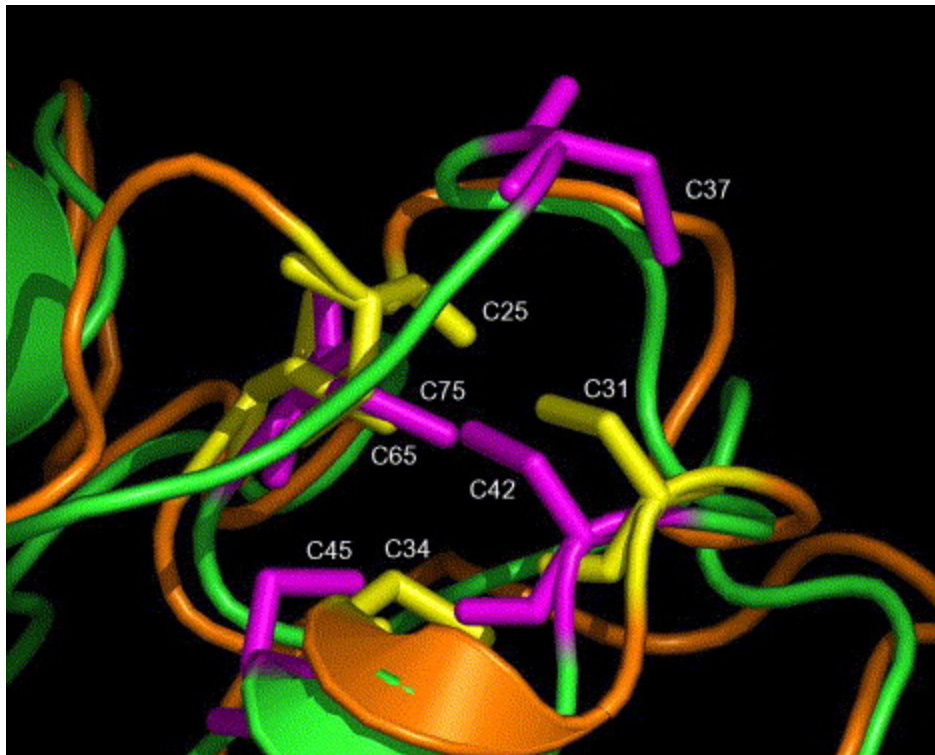
Fig. 4. The close view of the geometry of four cysteine residues bound to the redox [Fe2S2] center for the averaged structures from the AWD model (cysteines in magenta) and the JEV model (cysteines in yellow).

Table 1. Inter-atomic distances between sulfur atoms in the cysteine residues involved in the redox center in crystal structure (1awd), the AWD model and the JEV model

Inter-atomic distance (S–S)	Crystal structure (Å)	AWD model (Å) (averaged)	JEV model (Å) (averaged)
Cys75 (65)–Cys42 (31)	6.59	3.43	4.62
Cys37 (25)–Cys45 (34)	6.59	8.66	5.10
Cys75 (65)–Cys37 (25)	5.16	7.06	3.59
Cys37 (25)–Cys42 (31)	3.68	4.89	4.37
Cys45 (34)–Cys42 (31)	5.84	3.81	4.74
Cys45 (34)–Cys75 (65)	3.63	3.45	4.34

Note: residue numbers in parenthesis correspond to the residue numbers in JEV model while those outside the parenthesis represent the residue numbers in crystal structure and AWD model average structure.

This is the first report of a potential selenoprotein homologue of ferredoxin in any organism. However, ferredoxin–thioredoxin reductases are known to exist in some organisms, and in mammals thioredoxin reductases are selenoproteins. Thus a link between ferredoxin and selenium, in the form of a selenoprotein homologue of ferredoxin, does not seem unreasonable. Selenium and selenoproteins are critical regulators of cellular redox systems that control gene expression and apoptosis in cells of the immune system, so viruses may benefit from modulating the cellular selenium based redox enzyme systems.

This hypothesis is also consistent with the observations that TNF levels were elevated in the serum from JEV infected patients. It is also supported by the fact that in hepatitis C virus infected hosts, an increase of iron storage is believed to promote free-radical-medicated

peroxidation (via the Fenton reaction) and thereby cause liver damage. Since hepatitis C virus and JEV are from the same family of Flaviviridae, there might be an analogous link between iron and JEV. Comparison of the active site cysteines for both models in MD simulations reveals that the JEV model, with selenium in place of sulfur, may be helpful in stabilizing and maintaining the geometry of the [Fe2S2] redox core. Because of the physico-chemical properties of selenium, a selenocysteine-containing [Fe2S2] cluster would have slightly longer bond distances, which may exhibit red-shifted absorption bands, less negative redox potentials and larger paramagnetism. These properties will cause redox potential differences, which are an important driving force for electron transfer.

It is also worth noting that analogous observations might also exist in other human flaviviruses, such as dengue virus and West Nile virus, which also appear to encode selenoproteins in the NS4 gene regions. Our analysis suggests that a homologous hypothetical ferredoxin-like selenoprotein could be encoded in the −1 frame of the dengue virus NS4 region (data not shown). In both JEV and dengue virus, these ferredoxin-like selenoproteins could play a role in the electron transfer processes related to ROS, which are believed to be a major factor in liver damage. The liver damage observed in dengue virus and JEV infection is believed to be mediated either via the mechanism of the NF-κB/TNF-α pathway [27], [28] or via a network of cytokines, including the cytokine RANTES [29], [30]. Avirutnan et al. [31] showed that infection of human endothelial cells with Dengue virus induces the transcriptional up-regulation and the secretion of RANTES and IL-8. The chemokine RANTES (regulated upon activation, normal T cell expressed and secreted) belongs to the beta-chemokine family and is a chemoattractant for CD4+/CD45RO T cells [32]. RANTES has recently been shown to suppress replication of macrophage-tropic strains of HIV in CD4+ T cells [32]. RANTES expression has been observed during type II dengue virus infection of human endothelial cells, along with chemokine production, complement activation, and apoptosis [31]. Because ROS are mediators of these processes, it is possible that expression of this hypothetical ferredoxin-like selenoprotein in JEV and dengue virus might have benefit for the replication and survival of these flaviviruses.

4. Conclusions

In summary, we have identified a new overlapping gene in the JEV NS4B region with three highly conserved in-frame UGA codons, which may encode a novel selenoprotein homologue of ferredoxin. The fact that this peptide sequence is highly conserved in JEV isolates indicates the importance of this hypothetical gene. The modeled structure of this hypothetical protein is predicted to be energetically favorable and is predicted to have very close relationship to the 1awd ferredoxin structure. The RMSDs between the averaged structures of JEV model and AWD model is 1.83 Å in the aligned regions. The MD simulations data also indicate that this hypothetical JEV model could be quite stable at room temperature. From all the evidence available, we predict this protein might have a role in the JEV infection and replication via TNF, iron, and other cellular stimuli. Our research also indicates that the replacement of cysteine residues with selenocysteine residues might assist in maintaining the conformation of the [Fe2S2] cluster center, an important active site for electron transfer.

The real structure and function of the NS4B region of JEV, and its roles in virus infection remain to be solved. Given the structural feasibility and stability of the viral ferredoxin homolog as

discussed above, such biochemical experiments would be of considerable interest. If this gene proves to be functional, it would shed new light on the understanding of the pathogenic mechanism as well as new approaches to the prevention and treatment of infection by JEV and other Flaviviridae.

Acknowledgments

Appendix A. Supplementary material

Supplementary data associated with this article can be found online at https://doi.org/10.1016/j.jmgm.2004.07.002.

References

[1] K. Venugopal, E.A. Gould, Towards a new generation of flavivirus vaccines, Vaccine 12 (1994) 966–975.

[2] V. Ravi, S. Parida, A. Desai, A. Chandramuki, M. Gourie-Devi, G.E. Grau, Correlation of tumor necrosis factor levels in the serum and cerebrospinal fluid with clinical outcome in Japanese encephalitis patients, J. Med. Virol. 51 (1997) 132–136.

[3] R.F. Grimble, Nutritional modulation of cytokine biology, Nutrition 14 (1998) 634–640.

[4] M. Roederer, F.J. Staal, S.W. Ela, L.A. Herzenberg, N-acetylcysteine: potential for AIDS therapy, Pharmacology 46 (1993) 121–129.

[5] J.P. Merin, M. Matsuyama, T. Kira, M. Baba, T. Okamoto, Alphalipoic acid blocks HIV-1 LTR-dependent expression of hygromycin resistance in THP-1 stable transformants, FEBS Lett. 394 (1996) 9–13.

[6] E.W. Taylor, A. Bhat, R.G. Nadimpalli, W. Zhang, J. Kececioglu, HIV-1 encodes a sequence overlapping env gp41 with highly significant similarity to selenium-dependent glutathione peroxidases, J. Acquir. Immune Defic. Syndr. Hum. Retrovirol. 15 (1997) 393–394.

[7] R.A. Sunde, Selenium, in: B.L. O'Dell, R.A. Sunde (Eds.), Handbook of Nutritionally Essential Minerals, Marcel Dekker, New York, 1997, pp. 493–556.

[8] E.W. Taylor, A.G. Cox, L. Zhao, J.A. Ruzicka, A.A. Bhat, W. Zhang, R.G. Nadimpalli, R.G. Dean, Nutrition, HIV, and drug abuse: the molecular basis of a unique role for selenium, J. Acquir. Immune Defic. Syndr. 25 (Suppl. 1) (2000) 53–61.

[9] T.G. Senkevich, J.J. Bugert, J.R. Sisler, E.V. Koonin, G. Darai, B. Moss, Genome sequence of a human tumorigenic poxvirus: prediction of specific host response-evasion genes, Science 273 (1996) 813–816.

[10] J.L. Shisler, T.G. Senkevich, M.J. Berry, B. Moss, Ultraviolet-induced cell death blocked by a selenoprotein from a human dermatotropic poxvirus, Science 279 (1998) 102–105.

[11] F. Farinati, R. Cardin, N. De Maria, G. Della Libera, C. Marafin, P.E. Lecis, P. Burra, A. Floreani, A. Cecchetto, R. Naccarato, Iron storage, lipid peroxidation and glutathione turnover in chronic anti-HCV positive hepatitis, J. Hepatol. 22 (1995) 449–456.

[12] F. Farinati, R. Cardin, N. De Maria, P.E. Lecis, G. Della Libera, P. Burra, C. Marafin, G.C. Sturniolo, R. Naccarato, Zinc, iron, and peroxidation in liver tissue. Cumulative effects of alcohol consumption and virus-mediated damage—a preliminary report, Biol. Trace Elem. Res. 47 (1995) 193–199.

[13] W. Zhang, A.G. Cox, E.W. Taylor, Hepatitis C virus encodes a selenium-dependent glutathione peroxidase gene. Implications for oxidative stress as a risk factor in progression to hepatocellular carcinoma, Med. Klin. 94 (Suppl. 3) (1999) 2–6.

[14] L. Zhao, A.G. Cox, J.A. Ruzicka, A.A. Bhat, W. Zhang, E.W. Taylor, Molecular modeling and in vitro activity of an HIV-1-encoded glutathione peroxidase, Proc. Natl. Acad. Sci. U.S.A. 97 (2000) 6356–6361.

[15] GCG Wisconsin Package, Accelrys, San Diego, CA, URL: http://www.accelrys.com.

[16] National Center for Biotechnology Information, URL: http://www.ncbi.nlm.nih.gov.

[17] W. Zhang, C.S. Ramanathan, R.G. Nadimpalli, A.A. Bhat, A.G. Cox, E.W. Taylor, Selenium-dependent glutathione peroxidase modules encoded by RNA viruses, Biol. Trace Elem. Res. 70 (1999) 97–116.

[18] SYBYL, version 6.7, 2000, Tripos Inc., St. Louis, MO, URL: http://www.tripos.com.

[19] M.T. Bes, E. Parisini, L.A. Inda, L.M. Saraiva, M.L. Peleato, G.M. Sheldrick, Crystal structure determination at 1.4 A ° resolution of ferredoxin from the green alga Chlorella fusca, Structure Fold Des. 7 (1999) 1201–1211.

[20] D.A. Case, D.A. Pearlman, J.W. Caldwell, T.E. Cheatham III, W.S. Ross, C.L. Simmerling, T.A. Darden, K.M. Merz, R.V. Stanton, A.L. Cheng, J.J. Vincent, M. Crowley, D.M. Ferguson, R.J. Radmer, G.L. Seibel, U.C. Singh, P.K.Weiner, P.A. Kollman, AMBER 6, University of California, San Francisco, 1999, URL: http://amber.scripps.edu.

[21] W.D. Cornell, P. Cieplak, C.I. Bayly, I.R. Gould, K.M. Merz, D.M. Ferguson, D.M. Spellmeyer, T. Fox, J.W. Caldwell, P.A. Kollman, A second generation force field for the simulation of proteins, nucleic acids and organic molecules, J. Am. Chem. Soc. 117 (1995) 5179–5197.

[22] W.L. Jorgensen, J. Chandrasekhar, J.D. Madura, R.W. Impey, M.L. Klein, Comparison of simple potential functions for simulating liquid water, J. Chem. Phys. 79 (1983) 926–935.

[23] T. Darden, D. York, L. Pedersen, Particle mesh Ewald: an N log(N) method for Ewald sums in large systems, J. Chem. Phys. 98 (1993) 10089–10092.

[24] H.J.C. Berendsen, J.P.M. Postma,W.F. van Gunsteren, A. DiNola, J.R. Haak, Molecular dynamics with coupling to an external bath, J. Chem. Phys. 81 (1984) 3684–3690.

[25] Molecular Operating Environment (MOE), Version MOE 2002.03, 2002, Chemical Computing Group Inc., Montreal, Canada, URL: http://www.chemcomp.com.

[26] MidasPlus, 1995, Computer Graphics Lab, University of California, San Francisco, CA, URL: http://www.cgl.ucsf.edu/Outreach/midasplus.

[27] P. Marianneau, A. Cardona, L. Edelman, V. Deubel, P. Despres, Dengue virus replication in human hepatoma cells activates NFkappaB which in turn induces apoptotic cell death, J. Virol. 71 (1997) 3244–3249.

[28] P. Marianneau, M. Flamand, V. Deubel, P. Despres, Apoptotic cell death in response to dengue virus infection: the pathogenesis of dengue haemorrhagic fever revisited, Clin. Diagn. Virol. 10 (1998) 113–119.

[29] H. Liu, D. Chao, E.E. Nakayama, H. Taguchi, M. Goto, X. Xin, J.K. Takamatsu, H. Saito, Y. Ishikawa, T. Akaza, T. Juji, Y. Takebe, T. Ohishi, K. Fukutake, Y. Maruyama, S. Yashiki, S. Sonoda, T. Nakamura, Y. Nagai, A. Iwamoto, T. Shioda, Polymorphism in RANTES chemokine promoter affects HIV-1 disease progression, Proc. Natl. Acad. Sci. U.S.A. 96 (1999) 4581–4585.

[30] C.J. Chen, S.L. Liao, M.D. Kuo, Y.M. Wang, Astrocytic alteration induced by Japanese encephalitis virus infection, Neuroreport 11 (2000) 1933–1937.

[31] P. Avirutnan, P. Malasit, B. Seliger, S. Bhakdi, M. Husmann, Dengue virus infection of human endothelial cells leads to chemokine production, complement activation, and apoptosis, J. Immunol. 161 (1998) 6338–6346.

[32] H. Moriuchi, M. Moriuchi, A.S. Fauci, Nuclear factor-kappa B potently up-regulates the promoter activity of RANTES, a chemokine that blocks HIV infection, J. Immunol. 158 (1997) 3483–3491.